Front. Chem. Sci. Eng. 2019, 13(3): 511–516
https://doi.org/10.1007/s11705-019-1820-5

RESEARCH ARTICLE

Low-*k* integration: Gas screening for cryogenic etching and plasma damage mitigation

Romain Chanson (✉)[1], Remi Dussart[2], Thomas Tillocher[2], P. Lefaucheux[2], Christian Dussarrat[3], Jean François de Marneffe[1]

1 IMEC v.z.w., 3001 Leuven, Belgium
2 GREMI/University of Orleans, Orleans, France
3 Air Liquide Laboratories, Tsukuba, Japan

Abstract The integration of porous organo-silicate low-*k* materials has met a lot of technical challenges. One of the main issues is plasma-induced damage, occurring for all plasma steps involved during interconnects processing. In the present paper, we focus on porous SiOCH low-*k* damage mitigation using cryogenic temperature so as to enable micro-capillary condensation. The aim is to protect the porous low-*k* from plasma-induced damage and keep the *k*-value of the material unchanged, in order to limit the RC delay of interconnexion levels while shrinking the microchip dimension. The cryogenic temperature is used to condense a gas inside the porous low-*k* material. Then, the etching process is performed at the temperature of condensation in order to keep the condensate trapped inside the material during the etching. In the first part of this work, the condensation properties of several gases are screened, leading to a down selection of five gases. Then, their stability into the porous structure is evaluated at different temperature. Four of them are used for plasma damage mitigation comparison. Damage mitigation is effective and shows negligible damage for one of the gases at –50°C.

Keywords low-*k*, nanotechnology, micro-electronics, cryo-etching, plasma processing

1 Introduction

Nowadays, despite the introduction of metal with lower resistivity, scaling down in microelectronics requires materials with low-*k* value ($k < 3.0$). The main material family proposed for industrial reliability is porous organo-silicate glass (OSG). This material family allows dielectric constants below 3.0 by creating artificial porosity with a large interconnected network [1]. Unfortunately, their integration is an issue due to plasma-induced damage [2–4]. The dielectric material, after etching, becomes hydrophilic and absorbs moisture, which increases the *k*-value [5–8]. Different solutions have been proposed to mitigate damage during plasma processing [9–16]. The post porosity plasma protection (P4) was first proposed by IBM. This approach consists in stuffing the low-*k* by a sacrificial polymer. The latter is then removed after plasma process, metal filling and chemical mechanical planarization [11,12]. Although this approach shows good protection, it is discarded by the industry because of additional technical issues, such as the addition of four processing steps or the high thermal budget for polymer removal (up to 450°C). The plasma damage management is a pore grafting method. It does not protect the low-*k* material as well as the P4 solution [16]. The post damage, pore reparation CH_4-based plasma only works down to few nanometers deep and does not restore the low-*k* enough to be relevant for micro-electronics industry [9,10]. Cryo-etch was recently proposed as an alternative solution, and limit the need of additional steps to a single pore sealing step, after etch and before barrier deposition. It consists in condensing a gas into the porous structure before plasma ignition. The first proposed chemistry was a SF_6/C_4F_8 mixture. An efficient protection was demonstrated. However the technical issue was the need to work around a temperature of –120°C [13–15]. The capability to work above –50°C was demonstrated with a new reagent named high boiling point organic (HBPO), which was used with SF_6 first. It was demonstrated that the reaction between plasma by-products and methyl groups was reduced to negligible amount. Damage is propagating by vacuum

Received August 31, 2018; accepted January 28, 2019

E-mail: romain.chanson@gmail.com

ultraviolet (VUV) emission from the plasma and partially absorbed by the HBPO [17]. Additional experiments have also been performed with NF_3/HBPO chemistry. It was shown that some hydrogens of the methyl groups are removed but the Si−C bonds remain safe when HBPO is condensed into the low-*k*. Analysis after NF_3/HBPO etching showed that the low-*k* is safe in term of electrical and mechanical properties at –30°C and lower temperature [18]. In the present paper, we propose to continue the investigation to find a possible better reagent.

The paper is organized as follows: We first describe the tool set and methods used in this study. Then, the impact of wettability for condensation is demonstrated. These first results enable a first gas selection. Then, a phenomenon of large stability relative to the glass phase transition is shown for some of the tested gases. The evolution of both the etch rate and damage mitigation versus temperature is compared for the different reagents, correlated with measured *k*-values. Conclusions are given about the ability of the different condensed gases to protect the low-*k* from carbon depletion.

2 Experimental

In the present work, a SF_6/X gas mixture is used. X corresponds to one of the reagents screened for condensation into the porous low-*k*. The low-*k* material used for the contact angle measurement is a PECVD OSG-2.55 with pore diameter of 1.6 nm. For the etching experiments, a spin on glass (SOG-2.2) film with a pore diameter of 2.8 nm, a pristine *k*-value of 2.2 and a thickness of 200 nm, deposited on a 300 mm silicon wafer is used. 4×4 cm^2 coupons of blanket low-*k* films are glued on carrier wafers with a polyethylene glycol wax. Condensation and etching experiments is performed in a cryogenic-ICP alcatel 601E etching tool available at GREMI lab and already described in [13−15]. The reactor is also equipped with an additional liquid injection system. This system is a Bronkhorst controlled evaporator mixer connected by flow controllers to the vessel containing the re-agents, i.e., liquid HBPO, Sumida, Mikado or Akita (Air Liquide proprietary molecules). A carrier gas, which can be either SF_6, Ar, C_4F_8 or CF_4 is used to drive these products into the chamber. The density of the liquid HBPO, Sumida, Mikado or Akita is used to convert the mass flow from $g\cdot h^{-1}$ to sccm. The general conditions are as following: For condensation, the flow is $Q(SF_6/X)$ = 30/4 sccm, p = 22.5 mTorr, t = 1 min. For the etching process, $Q(SF_6/X)$ = 30/4 sccm, p = 22.5 mTorr, P_{rf} = 500 W, P_{DC} = 150 W, t = 1 min. The processing temperature is indicated in the text or in the figure. This reactor is also equipped with an ellipsometer from Jobin-Yvon, allowing *in-situ*, real-time film thickness and refractive index (RI) measurements. For this, the signal is fitted by a one layer Cauchy model and the RI at 633 nm is extracted. A single-layer model was considered relevant for the present system. The thickness is fixed for the condensation experiments (without etching). The effect of temperature was checked by performing thickness measurements between 20°C and –60°C, without condensation, showing no measurable change. This is consistent with the coefficient of thermal expansion of the SOG-2.2 film, which is ~34 $ppm\cdot°C^{-1}$, leading to an estimated thickness reduction of ~0.5 nm over T = 80°C. In addition, the impact of pore filling was investigated at –50°C with HBPO, no measurable difference were notified. So, we can safely estimate that the film shrinkage or swelling upon cooling and/or condensation has a negligible contribution to the RI change observed in this work. The RI change is therefore mainly caused by a density increase. When experiments took place, measurements in kinetic mode were not available due to technical problems. For post plasma analysis, a Nicolet FT-IR spectrometer is used to estimate the methyl depletion depth after plasma etching and annealing at 400°C under N_2 atmosphere. The low-*k* chemical composition was characterized at each step by Fourier-transform infrared spectroscopy (FT-IR) measurements using a Nicolet 6700® (Thermo Scientific) spectrometer in the wavenumber range 400−4000 cm^{-1}, 100-scans averaging with a resolution of 4 cm^{-1} in transmission mode. The FT-IR spectrometer allows for the measurement of the ratio of methyl depletion between the etched film and the pristine film. This ratio allows the calculation of the so-called equivalent damage layer (EDL). The concept of EDL was described in more details for the first time in [19]. Dielectric constant of the low-*k* films is determined from capacitance measured with an E4980A precision LCR (L for the inductance, C for capacitance and R for the resistance) meter on planar metal-insulator-semiconductor structures formed by the evaporation of 70 nm Platinum contact pads on top of n-Si/low-*k* stacks. Prior to *k* value extraction, or FT-IR measurements, annealing at 400°C under N_2 is performed. The aim is to remove the plasma by-products present after plasma exposure inside the low-*k*. More details about the interactions between the low-*k* and these by-products are given in [17]. Air Liquide measured the partial pressures for the different gases by the way of an isolated system allowing for local temperature stabilization of the liquid and measurement of vapor pressure as a function of the temperature. The wall of the device is constantly at higher temperature than the liquid. Air Liquide also measured the contact angle of the different candidates. Static contact angles were measured. Corresponding images were acquired using a contact angle measurement system equipped with an optical microscope (Olympus CKX41) coupled with a high-speed camera (Fastcam Ultima-512, Photron). Error margin is estimated to be ±3°.

3 Results and discussion

3.1 Wettability and condensation temperature

In this part, we establish a link between the wettability and the condensation behavior of the gases into the low-*k*. For this, the evolution of the contact angle is compared to with ΔT as defined thereafter. The condensation into the low-*k* is measured by *in-situ* ellipsometry, by recording the RI (evolution as a function of temperature).

We define ΔT as the difference between the temperature of condensation into the SOG-2.2 (T_{lk}) for a given partial pressure of the reagent and the temperature (T_A) measured at the same pressure (saturated vapor pressure) at Air Liquide (see experimental part). ΔT is defined as following in the Eq. (1):

$$\Delta T = T_{lk} - T_A. \quad (1)$$

Figure 1 shows the value of the contact angle and ΔT regarding the different reagents. The temperatures of condensation inside the low-*k* are measured by following the RI change every five degrees. One minute of stand-by is respected at each temperature in order to ensure that the system is in equilibrium. By considering the Lorenz-Lorentz equation with the RI of the low-*k*, the RI of the reagent and the ratio of porosity, we can determine that when the RI varies from 1.27 to 1.38, the full micro-capillary condensation is reached. For more details, see our previous publication on HBPO [17]. In the Fig. 1, we can see that the more the contact angle decreases, the more ΔT will increase. After this observation, we focused on the gases with the better wettability because, first, they condense above –50°C at a partial pressure of 2.5 mTorr. This low partial pressure is necessary to have the weakest proportion of reagent into the plasma discharge that will be used subsequently for pattern transfer. Also, working above –50°C is important for industrial applications. The second reason relates to the huge stability of some gases. This is why *iso*-propyl alcohol (IPA) was rejected: This molecule did not show this behavior. In the next part, two molecules from the same family than HBPO and Sumida will be introduced. These molecules have been introduced in this study in the last moment and the partial pressure regarding the temperature was not measured. That is the reason why they did not appear in the Fig. 1.

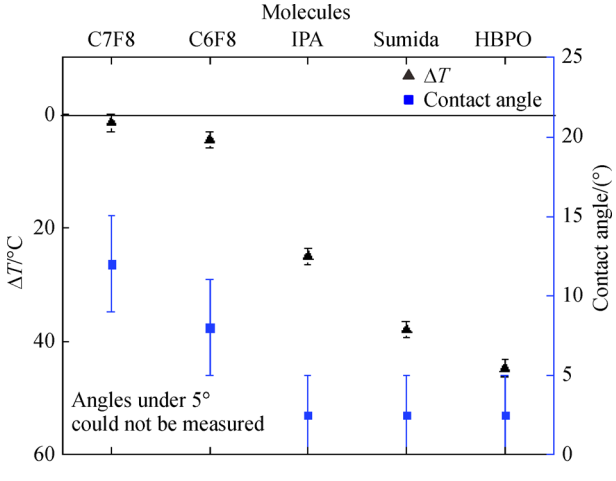

Fig. 1 Correlation of the evolution of ΔT, the difference between condensation temperature of different gases into SOG-2.2 and the temperature associated to the partial pressure of a gas, and contact angle of the different molecules on OSG-2.55.

3.2 High stability state

The stability of the condensate is evidenced by comparing the RI obtained from ellipsometry measurements made at different condensation temperatures in two different ways: First, from a measurement after condensation; second, by taking another measurement five minutes after removing the condensation reagent from the gas phase. The IPA does not show any stability even after decreasing the temperature until IPA condenses over the low-*k* surface (saturated vapor pressure). The other gases selected allow for a large stability after condensation owing to glass phase transition.

The stability area (SA) is defined as the temperature range corresponding to the stable condensed phase without reagent present in the gas phase for 5 min. The condensed phase is considered stable if the RI remains equal or higher than 1.35. This value corresponds to about 75% pore filling using Lorenz-Lorentz equation with a RI of 1.275 for these gases.

Figure 2 presents the RI of the OSG-2.2 as a function of temperature just after condensation (full symbols) and 5 min after pumping out the reagent (open symbols, SF_6 is kept alone in the medium during this period). For Sumida, we measure a high RI between –70°C and –55°C. This is due to intermediate state between micro-capillary condensation and the condensation of a film on top of the low-*k* layer. Indeed, for this experiment, the total film thickness was fixed in our Cauchy model. So, instead of fitting the signal with a higher thickness, the model fits with a higher RI. A slight increase is also observed between –40°C and –55°C. This phenomenon happens for the other reagents after condensation. This may be due to densification of the condensed phase while temperature decreases. When the temperature is too low, for all the gases, the ellipsometric signal becomes very noisy. Attempts to use a more complex model to fit this signal were not successful. This is the reason why the SA presents a maximum and minimum temperature. The formation rate of the condensate, its state and density cannot be studied by our system. We have only observed that working at temperature under the SA prevents the etching of the low-*k*.

In Fig. 2(a), Sumida shows a SA from –70°C to –50°C. Nevertheless, working under –55°C does not allow for a good control of the condensation process and, as a

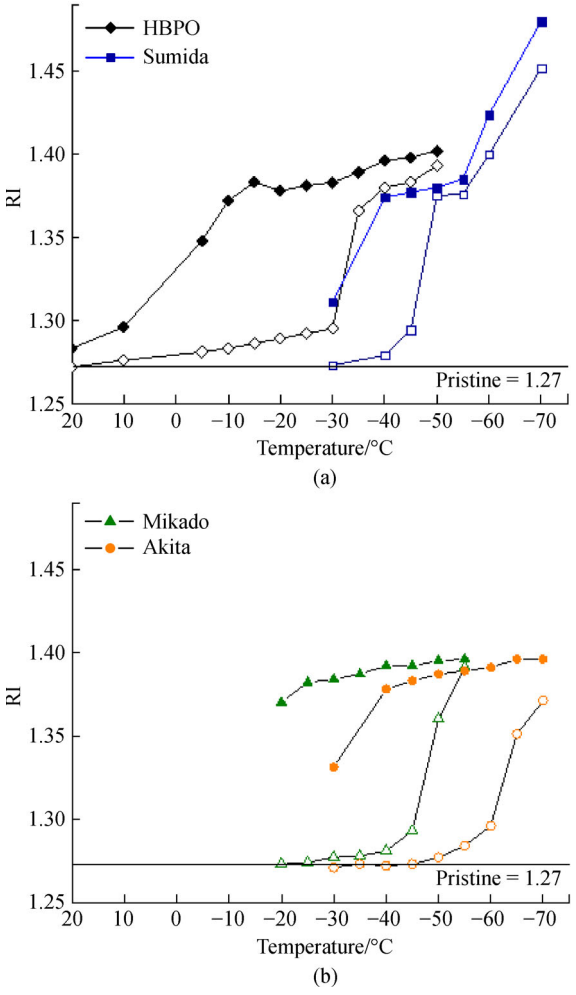

Fig. 2 Stability of (a) HBPO and Sumida, (b) Mikado and Akita. Full symbol is the RI after condensation and before pumping out of gas, open symbols show the RI 5 min after pumping out the reagent.

consequence, of the etching process. The HBPO shows a SA between –55°C and –35°C. These two reagents show a very good stability since the RI after condensation and five minutes after condensation is nearly identical. In the Fig. 2(b), Akita shows a SA from –70°C to –65°C. The Mikado shows a SA from –55°C to –50°C. At –55°C, Mikado shows a very good stability but the RI drops from 1.39 to 1.36 close to the limit value of 1.35 that was defined before. Akita is always less stable, dropping from 1.39 to 1.37 at –70°C and from 1.39 to 1.35 at –65°C.

In terms of stability, HBPO and Sumida show the larger SA with the lower variation of RI after 5 min of condensation. Nevertheless, both these candidates can be considered as interesting for damage mitigation since they condensate over –50°C.

3.3 Damage mitigation

We have shown in [17] that methyl depletion is directly related to damage, leading to moisture uptake and *k*-value increase. Without condensation, the synergy between the VUV emission and the by-products leads to a significant increase of the damage, much more than each effect taken separately [20]. Conversely, when the HBPO is condensed, the damage is mainly induced by plasma-induced VUV radiation scissioning of the $Si{-}CH_3$ bonds, and the reactions with plasma radicals can be neglected [17]. After condensation, the other gases presented here must show the same general behavior since their chemical formulae is close to the one of HBPO. This paragraph will describe whether or not the stability of the reagent can help to protect efficiently the low-*k* material. For this, all the gases will be used at the limit of their SA.

Once the reagent condensed in the pores, the low-*k* material is etched by an SF_6-based plasma. In Fig. 3, full symbols shows the average etch rate during a 1 min long plasma exposure with 150 W RF bias, using the discharge conditions described in the experimental section. The temperature selection for the different candidates is defined as follows: Each sample is etched at 20°C as a reference of damage before the condensation is initiated for pore protection. Then, the highest temperature in the SA is used. Etch rate decreases with temperature. Etch rates are above 110 $nm \cdot min^{-1}$ at 20°C for all the gases. At the lowest used temperature, the etch rate with SF_6/Akita plasma is still around 100 $nm \cdot min^{-1}$, SF_6/HBPO around 80 $nm \cdot min^{-1}$. The lowest etch rates are obtained for SF_6/Mikado and SF_6/Sumida plasma around 60 $nm \cdot min^{-1}$. All these etch rates are compatible with process requirements of the micro-electronics industry.

Open symbols of Fig. 3 correspond to the damage depth measured in the same conditions for the different molecules. The highest EDL is obtained for the HBPO at

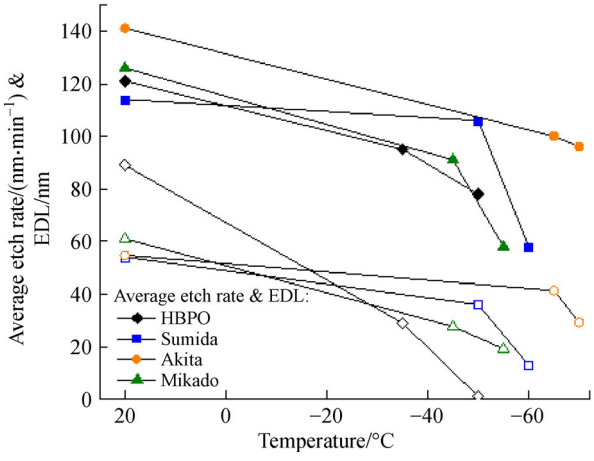

Fig. 3 Full symbols: Average etch rate measured as a function of the substrate temperature with the different reagents. Open symbols correspond to the damage depth estimated by the method of EDL, plasma conditions were $Q(SF_6/X)$ = 30/4 sccm, p = 22.5 mTorr. P_{rf} = 500 W, P_{DC} = 150 W bias. The temperature is indicated in the figure (X still represents one of the reagent).

room temperature. At the highest temperature of the SA, the HBPO and Mikado show the best values for damage (mitigation with an EDL of around 28 nm). The EDL are around 35 nm for Sumida and 40 nm for Akita. At the lower temperature of their SA, Sumida and HBPO show the lowest EDL, respectively 13 nm and zero (negligible damage, within error bars). For Mikado, the minimum EDL is around 20 nm. For Akita, the minimum EDL is around 30 nm.

Figure 4 shows the extracted *k*-values of the films versus the substrate temperature. The *k*-values for Akita at 20°C and HBPO at –35°C are higher than expected if we consider the EDL only: These two samples were probably damaged during transportation.

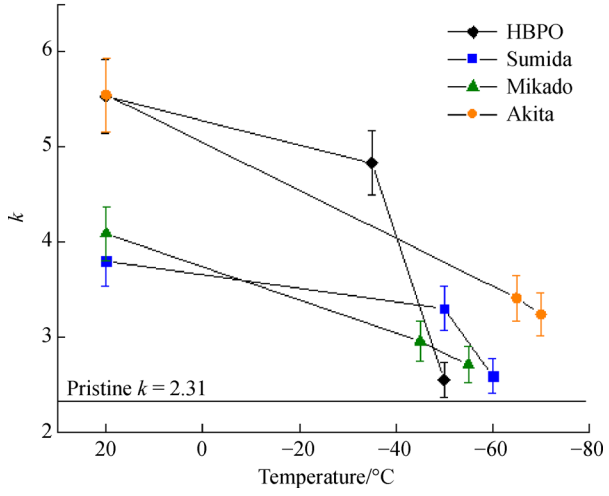

Fig. 4 *k*-value of the SOG-2.2 films after etching at different temperatures with the different reagents.

The best values obtained at 20°C are around 4 instead of 2.3 for the pristine sample. At this temperature, the low-*k* is not protected by condensed molecules. Damage is driven by VUV and by reaction with plasma by-products, which explains the degradation of the electrical properties. At the higher SA temperature, the *k*-values of Sumida and Mikado are around 3−3.2. The etching temperature is –45°C for Mikado and –50°C for Sumida. For Akita the value is close to 3.5. At this temperature, the glassy condensed phase may phase a lower protection than at lower temperature. Indeed, the condensed phase can become liquid if the interactions with the plasma induce warming up of the surface. At lower temperature, the solid phase is denser and protects better the low-*k*. After etching at the lowest temperature of the SA, the measured *k*-values reach their lowest value (closer to the pristine) for all the samples. Akita shows the highest *k*-value amongst all: Around 3 at –70°C. The HBPO, Mikado and Sumida show the best values, close to 2.5 at respectively –50°C, –55°C and –60°C. This is correlated to the low EDL calculated for these samples. In terms of temperature window for low damage and *k*-value, the HBPO shows slightly better results than Mikado or Sumida. Nevertheless, Mikado and Sumida have also to be considered since they show also good protection. Despite the protection is worse for Akita, the gas showing the lowest stability after condensation into the low-*k*, the link between the condensate stability and the protection is not so clear. In one hand, Mikado presents a similar protection as Sumida, but with a lower stability window. Also, protection at the coldest temperature seems to be better for all the reagents probably due to a denser condensed phase. More in-depth studies have to be performed to clarify this point. Nevertheless, this first data set should entice new studies for cryogenic low-*k* patterning in back end of line.

4 Conclusions

In the present work, we have compared the condensation behavior of seven reagents. Among those, stability tests were performed for five gases allowing condensation above –50°C. Four candidates have shown high stability due to glass phase transition. HBPO and Sumida show a large stability window, in comparison to Mikado and Akita. All these gases have been studied for damage mitigation during the plasma etching of a SOG-2.2 ultra-porous low-*k* material. The etch rates, for all the gases, at all investigated temperatures, are found to be fast enough for micro-electronics standard of integration. The HBPO, Sumida and Mikado present the best damage mitigation properties, whereas significant damage remains with Akita. The EDL is well linked to the measured post-etch *k*-values. The *k*-values are found to be very close to the pristine (2.31) for HBPO, Mikado and Sumida at –50°C, –55°C and –60°C, respectively.

Because a substrate temperature equal or above –50°C must be used for industrial process, the HBPO molecule is the best candidate of all gases. Low-*k* materials with higher

Table 1 Bests reagents found for plasma etching damage mitigation in SOG-2.2 as low-*k* (average pores Ø = 2.8 nm)

Reagent	Condensation temperature/°C	SA/°C	Etch rate/(nm·min^{-1}) [a)]	EDL/nm [b)]	*k* value [c)]
HBPO	–20	20 (–35 → –50)	78	0	2.55
Sumida	–40	10 (–50 → –60)	58	13	2.71
Mikado	–30	5 (–45 → –50)	55	19	2.59
Akita	–50	0–5 (–65 → –70)	96	29	3.24

a) At the better temperature for damage mitigation; b) Lower value; c) Lower value

k-values have typically lower porosity and lower pore radius. For smaller pores, the phenomena of micro-capillary condensation and glass phase transition will take place at higher temperature, leading to a protection occurring at higher temperature. For such materials, the use of Mikado or Sumida may be considered as well. The Table 1 gives a summary of the present gas set comparison.

Acknowledgements The authors acknowledge Dr. P. Shen and K. Urabe from Air Liquide Laboratories for providing HBPO, Sumida, Mikado and Akita molecules. This project has received funding from the European Union's Horizon 2020 research and innovation program under the Marie Sklodowska-Curie grant agreement No. 708106.

References

1. Maex K, Baklanov M R, Shamiryan D, Lacopi F, Brongersma S H, Yanovitskaya Z S. Low dielectric constant materials for microelectronics. Journal of Applied Physics, 2003, 93(11): 8793–8843
2. Baklanov M R, Vanhaelemeersch S, Bender H, Maex K. Effect of oxygen and fluorine on the dry etch characteristics of organic low-*k* dielectrics. Journal of Vacuum Science & Technology B, 1999, 17 (2): 372–380
3. Baklanov M R, Mogilnikov K P, Le Q T. Quantification of processing damage in porous low dielectric constant films. Microelectronic Engineering, 2006, 83(11-12): 2287–2291
4. Shamiryan D, Baklanov M R, Vanhaelemeersch S, Maex K. Comparative study of SiOCH low-*k* films with varied porosity interacting with etching and cleaning plasma. Journal of Vacuum Science & Technology B, 2002, 20(5): 1922–1929
5. Lepinay M, Lee D, Scarazzini R, Bardet M, Veillerot M, Broussous L, Licitra C, Jousseaume V, Bertin F, Rouessac V, Ayral A. Impact of plasma reactive ion etching on low dielectric constant porous organosilicate films' microstructure and chemical composition. Microporous and Mesoporous Materials, 2016, 228: 297–304
6. Humbert A, Mage L, Coldberg C, Junker K, Proenca L, Lhuillier J B. Effect of plasma treatment on ultra low-*k* material properties. Microelectronic Engineering, 2005, 82(3-4): 399–404
7. Ren H, Antonelli G A, Nishi Y, Shohet J L. Plasma damage effects on low-*k* porous organosilicate glass. Journal of Applied Physics, 2010, 108(9): 094110
8. Kunnen E, Baklanov M R, Franquet A, Shamiryan D, Rakhimova T K, Urbanowicz A M, Struyf H, Boullart W. Effect of energetic ions on plasma damage of porous SIOCH low-*k* materials. Journal of Vacuum Science & Technology B, 2010, 28: 448–459
9. Singh S K, Kumbhar A A, Dusane R O. Repairing plasma-damaged low-*k* HSQ films with trimethylchlorosilane treatment. Materials Science and Engineering B, 2005, 127(1): 29–33
10. Shi H, Bao J, Huang H, Ho P S, Goodner M D, Moinpour M, Kloster G-M. Effect of CH_4 plasma treatment on O_2 plasma ashed organosilicate low-*k* dielectrics. Matererial Research Society Proceeding B, 2007, 990: 51–56
11. Frot T, Volksen W, Magbitang T, Miller D C, Purushothaman S, Lofaro M, Bruce R, Dubois G. Post porosity plasma protection a new approach to integrate $k \leqslant 2.2$ porous ULK materials. In: IEEE International Interconnect Technology Conference, 2011. New York: IEEE, 2011
12. Frot T, Volksen W, Purushothaman S, Bruce R, Dubois G. Application of the protection/deprotection strategy to the science of porous materials. Advanced Materials, 2011, 23(25): 2828–2832
13. Leroy F, Zhang L, Tillocher T, Yatsuda K, Maekawa K, Nishimura E, Lefaucheux P, de Marneffe J F, Baklanov M R, Dussart R. Cryogenic etching processes applied to porous low-*k* materials using SF_6/C_4F_8 plasmas. Journal Physics D, 2015, 48(43): 435202
14. Zhang L, de Marneffe J F, Leroy F, Lefaucheux P, Tillocher T, Dussart R, Maekawa K, Yatsuda K, Dussarrat C, Goodyear A, Cooke M, De Gendt S, Baklanov M R. Mitigation of plasma-induced damage in porous low-*k* dielectrics by cryogenic precursor condensation. Journal Physics D, 2016, 49(17): 175203
15. Zhang L, Ljazouli R, Lefaucheux P, Tillocher T, Dussart R, Mankelevich Y A, de Marneffe J F, De Gendt S, Baklanov M R. Damage free cryogenic etching of a porous organosilica ultralow-*k* film. ECS Solid State Letters, 2013, 2(5-N): 7
16. Rezvanov A, Zhang L, Watanabe M, Krishtab M B, Zhang L, Hacker N, Verdonck P, Armini S, de Marneffe J F. Pore surface grafting of porous low-*k* dielectrics by selective polymers. Journal of Vacuum Science & Technology B: Microelectronics and Nanometer Structures, 2017, 35: 021211
17. Chanson R, Zhang L, Naumov S, Mankelevich Yu A, Tillocher T, Lefaucheux P, Dussart R, De Gendt S, De Marneffe J F. Damage-free plasma etching of porous organo-silicate low-*k* using micro-capillary condensation above −50°C. Scientific Reports, 2018, 8(1): 1886)
18. Chanson R, Tahara S, Vanstreels K, de Marneffe J F. Low damage ultra-low-*k* patterning using a high boiling point organic (HBPO) combined with NF_3. Plasma Research Express, 2018, 1(1): 015006
19. Darnon M, Casiez N, Chevolleau T, Dubois G, Volksen W, Frot T J, Hurand R, David T L, Posseme N, Rochat N, et al. Impact of low-*k* structure and porosity on etch processes. Journal of Vacuum Science & Technology B, 2013, 31: 011207
20. Zotovich A, Rezvanov A, Chanson R, Zhang L, Hacker N, Kurchikov K, Klimin S, Zyryanov S M, Lopaev D, Gornev E, et al. Low-*k* protection from F radicals and VUV photons using a multilayer pore grafting approach. Journal of physic D, 2018, 51: 325202